View metadata, citation and similar papers at core.ac.uk

brought to you by CORE

provided by Qatar University Institutional Repository

coatings

MDPI

Article

Novel Electrodeposited Ni-B/Y_2O_3 Composite Coatings with Improved Properties

Rana Abdul Shakoor [1,*], Umesh Somaji Waware [1], Kamran Ali [1,2], Ramazan Kahraman [3], Anton Popelka [1], Moinuddin Mohammed Yusuf [1] and Anwarul Hasan [4]

1 Center for Advanced Materials, Qatar University, P.O. Box 2713, Doha, Qatar; uswaware@qu.edu.qa (U.S.W.); kamran_ali1214@yahoo.com (K.A.); anton.popelka@qu.edu.qa (A.P.); moinuddin@qu.edu.qa (M.M.Y.)
2 Department of Mechanical Engineering, DHA Suffa University, Karachi-75500, Pakistan
3 Department of Chemical Engineering, College of Engineering, Qatar University, P.O. Box 2713, Doha, Qatar; ramazank@qu.edu.qa
4 Department of Mechanical and Industrial Engineering, College of Engineering, Qatar University, P.O. Box 2713, Doha, Qatar; ahasan@qu.edu.qa
* Correspondence: shakoor@qu.edu.qa; Tel.: +974-4403-6867

Received: 21 August 2017; Accepted: 26 September 2017; Published: 29 September 2017

Abstract: Ni-B/Y_2O_3 composite coatings were developed through an electrodeposition process to study the effect of addition of Y_2O_3 particles on structure, surface, thermal, mechanical, and anticorrosion properties of Ni-B coatings. It is revealed that parent crystal structure of Ni-B matrix is preserved by addition of Y_2O_3, however, a noticeable improvement in crystallinity is observed. The analysis of the surface exhibits formation of dense and nodular deposits in the two types of coatings, but incorporation of Y_2O_3 particles in Ni-B matrix has resulted in a noteworthy change in grain size and surface roughness. Thermal analysis of the surfaces indicates that Ni-B-Y_2O_3 composite coatings demonstrate superior thermal stability compared to Ni-B coatings. The nanoindentation analysis shows a significant enhancement in the mechanical characteristics of the Ni-B matrix by addition of Y_2O_3 particles. This may be contemplated as the result of grain refinement and dispersion hardening of the Ni-B matrix by the presence of hard Y_2O_3 particles. A decent improvement in the corrosion protection efficiency (73.6%) is also observed by addition of Y_2O_3 particles into Ni-B matrix. Simultaneous improvement of mechanical and anticorrosion properties suggests potential applications of Ni-B-Y_2O_3 coatings in oil and gas, automobile, and many other industries.

Keywords: electrodeposition; composite coating; grain size; crystalline; hardness; nanoindentation; corrosion

1. Introduction

Wear and corrosion usually act together leading to significant damage in various industrial applications such as chemical and mineral processes, mining, pulp/paper, and the energy industry [1]. Material damage control by surface protection techniques by applying coatings of some suitable materials has proven to be effective [2]. Among various types of coatings, composite coatings have attracted attention due to their decent merits such as protection against corrosion, wear, and improved microhardness relative to pure metallic or alloy coatings. Aqueous metal deposition techniques like electroless plating or electro-deposition have gained considerable attentiveness because of their impressive superiority such as simpler operation, low cost, high deposition rate, uniformly deposited layers, and good wear and corrosion properties [3,4]. Ni-B coatings are famous for their excellent wear resistance and high hardness coupled with decent characteristics like durability, uniformity of layer thickness, lubricity and ductility, exceptional solderability, decent electrical characteristics, antimicrobial properties, low porosity, excellent bonding, electromagnetic

characteristics, etc. [5,6]. Due to these attractive characteristics, Ni-B coatings have found multiple uses in automotive, aeronautics, nuclear, astronautics, petrochemical, electronic devices, plastics, optics, textile, paper/pulp, food, and print industries [7–9].

It was recently observed that electrodeposited Ni-B matrix is fairly suited to accommodate incorporated second phase particles resulting in improved hardness and excellent wear endurance [1,2,10,11]. A decent number of reports have been published on the application of insoluble and hard reinforcements into Ni-B matrix including TiO_2 [11,12], CeO_2 [2], ZrO_2 [8], Al_2O_3 [1], SiC [13], Si_3N_4 [7,10], and mixed oxide reinforcement ZrO_2-Al_2O_3 [4]. To the best of our knowledge, the result of application of Y_2O_3 particles on the characteristics of Ni-B coatings has not been yet investigated. We have selected Y_2O_3 to reinforce Ni-B matrix because of its characteristics such as good thermal and chemical stability, insolubility in water and promising effects on structure, mechanics (wear resistance and hardness) and corrosion endurance.

The study at hand is concerned with understanding the influence of incorporation of Y_2O_3 particles on structure, surface, thermal, mechanical, and anticorrosion properties of Ni-B matrix. A significant effect on structural, surface, thermal, mechanical, and anticorrosion properties is noted by the addition of Y_2O_3 particles to the Ni-B matrix. The encouraging role of Y_2O_3 particles addition to Ni-B matrix enables Ni-B-Y_2O_3 composite coatings to demonstrate superior properties when compared to Ni-B and thus make these novel coatings attractive for oil and gas, automobile, seawater desalination, and many other industries.

2. Materials and Methods

2.1. Sample Preparation

Ni-B and Ni-B-Y_2O_3 composite coatings were prepared using the electrodeposition process. Polished mild steel samples (30 mm × 30 mm × 1.5 mm) were used as substrates having composition (wt %) of 0.186, 0.214, 0.418, 0.029, and 0.019 for carbon, silicon, manganese, phosphorous, and sulphur, respectively. Mechanical grinding and polishing was done using different silicon carbide abrasive papers (220 to 1200 grit size). After cleaning with an alkaline solution, prepared substrates were sonicated in acetone for 30 min. Finally, the substrate surfaces were activated in freshly prepared 20% solution of HCl for one minute to remove the last traces of any surface contamination. The substrates were then washed with distilled water. The edges and one face of the samples were masked with epoxy tape so that the electrodeposition of coatings can be confined to one selected face. To proceed with the deposition, the mild steel substrates were connected to the negative (cathode) and nickel plate to the positive (anode) poles of the DC power supply. The analysis of coating baths (Bath 1 and Bath 2) and operating parameters for Ni-B, and Ni-B-Y_2O_3 composite coatings are summarized in Table 1. The coating bath composition is based on the well-known Watts Nickel Bath solution which contains nickel chloride, nickel sulfate, and boric acid. Boric acid is intended to control the pH of the salt bath, and the dimethylamine borane complex is utilized as the source for boron. In the case Ni-B-Y_2O_3 coatings, an optimized concentration of 9 g/L was used for Y_2O_3 particles, whereas; the coating deposition was carried out at 45 ± 1 °C for 30 min. In order to prevent the sedimentation and agglomeration of Y_2O_3 particles, the composite coating bath was vigorously agitated at 500 rpm with magnetic stirrer. The coating bath was subjected to constant agitation using a magnetic stirrer for one hour before the start of the coating process to ensure uniform dispersion of the particles.

Table 1. Coating bath composition and operating parameters.

Chemicals	Bath 1 (Ni-B)	Bath 2 (Ni-B-Y_2O_3)
Nickel sulfate hexahydrate	240 g/L	240 g/L
Nickel chloride hexahydrate	45 g/L	45 g/L
Boric acid	30 g/L	30 g/L
Dimethylamine borane complex	3 g/L	3 g/L
Y_2O_3 powder particles (micron size)	–	9.0 g/L
pH	4 ± 0.2	4 ± 0.2
Temperature	45 ± 1 °C	45 ± 1 °C
Deposition time	30 min	30 min
Current density	50 mA/cm^2	50 mA/cm^2
Bath agitation	500 rpm	500 rpm

2.2. Sample Characterization

Properties of the developed coatings were studied and analyzed through various characterization techniques. X-ray diffractometer (XRD, Rigaku, Miniflex2 Desktop, Tokyo, Japan) was used to study the crystal structure of the coatings by employing Cu Kα radiations. Diffraction patterns were recorded at a scanning step of 0.02°. The coating morphology (grain size, shape, distribution, etc.) was studied using field emission scanning electron microscope (FE-SEM, FEI, Nova Nano-450, Eindhoven, The Netherlands) and surface characteristics (texture, roughness) were investigated with atomic force microscopy (MFP-3D AFM, Asylum Research, Santa Barbara, CA, USA). Compositional analysis of synthesized coatings was done through energy dispersive X-ray spectroscopy coupled with field emission scanning electron microscope. Thermal stability of synthesized coatings was investigated in the temperature range of 25–450 °C by differential scanning calorimetry (DSC, JADE, Perkin Elmer, Shelton, CT, USA) in the presence of argon. Mechanical properties (hardness, Young's modulus) of the developed coatings were determined using MFP-3D Nanoindenter coupled with atomic force microscopy. A standard tip indenter with a spring constant of 4000 N/m was used in our study. The nanoindentation was carried out by employing Berkovich diamond indenter tip using a maximum 1 mN indentation force (loading and unloading rate: 200 μN/s, dwell time at maximum load: 5 s) and the resultant contact penetration from the unloading curve was determined using Oliver and Pharr method. Corrosion tests were conducted using a three electrode flat electrochemical cell reported elsewhere [14]. Graphite was used as counter electrodes, saturated calomel as reference electrodes, and steel substrates as working electrodes to study the electrochemical behavior of Ni-B, and Ni-B-Y_2O_3 composite coatings. Deaeration was carried out before the initiation of each corrosion test using nitrogen gas for 2 h to flash out any contaminant gas that may have existed in the test cell. NaCl was used as the corrosion medium with 3.5% concentration and a saturation pH value of 7.2 was achieved. Corrosion tests were performed at ambient temperature. Potentiodynamic polarization experiments were carried out using a Gamry Reference Eco potentiostat at a scan rate of 10 mV·min^{-1} (0.167 mV·s^{-1}) using fixed exposed area of 0.785 cm^2. All measurements were done at room temperature.

3. Results and Discussion

3.1. Structural and Compositional Analysis

Structural analysis and phase purity of pure Ni-B and Ni-B-Y_2O_3 composite coatings in their as synthesized state are shown in Figure 1. The large scale XRD scans with 2θ range (40°–110°) for Ni-B and Ni-B-Y_2O_3 composite coatings have been presented in Figure 1a, whereas the small scale scan with 2θ range (40°–60°) is presented in Figure 1b for a clear comparison. The absence of any undesired peaks indicates the synthesis of phase pure coatings.

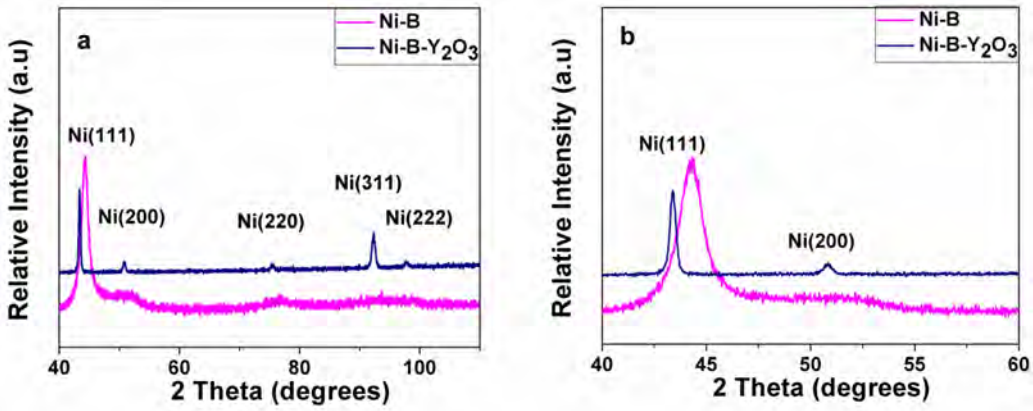

Figure 1. The large (**a**), and small scale (**b**) XRD spectra of electrodeposited Ni-B and Ni-B-Y_2O_3 composite coatings.

The small scale XRD pattern i.e., 2θ range (40°–60°) clearly demonstrates the peak shifting and broadening of peak (111) in the XRD scan. As illustrated, the XRD spectra of Ni-B show a single broad Ni (111) peak at 2θ (~45°) depicting its semi amorphous crystal structure. However, additional reflections of Ni (200), Ni (220), Ni (222), and Ni (311) are clearly visible in the XRD spectrum of Ni-B-Y_2O_3 composite coatings. Unlike Ni-B coating, sharp peaks in Ni-B-Y_2O_3 composite coatings reveal the crystalline nature of the composite layer. This result supports the earlier reported findings that the co-deposition of hard ceramic particles improve the crystallinity of the Ni-B matrix [1,2]. Furthermore, shifting of Ni (111) main peak towards lower 2θ value (~43°) indicates the expansion of the unit cell confirming the co-deposition of Y_2O_3 particles into Ni-B matrix. It is anticipated that incorporation of Y_2O_3 particles having relatively large size results in misfit into the matrix. This mechanism creates strain and causes expansion of the matrix. The expansion leads to the shifting of 2θ values towards lower range. The crystallinity of nickel is improved because of the reason that Y_2O_3 particles itself are of crystalline phase. The incorporation of high crystalline phase results in high accumulative intensity of nickel phase. The grain size of the synthesized coatings was calculated by the following Scherrer equation [5,15]. The diffraction peak of Ni (111) was used to calculate the grain size (see Equation (1)).

$$L = K\lambda/(\beta\ (2\theta) \times \cos\theta) \quad (1)$$

In this equation, L is the mean grain size of the phase and K is the shape factor which is a dimensionless quantity. The shape factor has a usual value of about 0.9 and changes with the real shape of the crystallites, X-ray wavelength is shown with λ (1.54060 Å), line broadening at half of the maximum intensity (FWHM) is β, and θ is the Bragg angle (in degrees). A comparison of grain size measurement indicates that Ni-B coatings (~10 nm) have large grain size compared to Ni-B-Y_2O_3 composite coatings (~6 nm) and concludes that the incorporation of Y_2O_3 particles into the Ni-B matrix refines its grain. The refinement in grain size might be attributed to the hard and insoluble Y_2O_3 particles. Incorporation of Y_2O_3 particles provide numerous heterogeneous nucleation sites throughout the Ni-B matrix and blocks the grain growth [16,17].

The co-deposition of both boron (B) and yttria (Y_2O_3) into nickel (Ni) matrix was also confirmed with EDX analysis and the results are presented in Figure 2.

Incorporation of both boron (B) and Y_2O_3 particles into nickel matrix is clearly recognized, resulting in the formation of Ni-B and Ni-B-Y_2O_3 composite coatings. It can be observed that nickel, boron, and yttrium peaks are detected in the Ni-B and Ni-B-Y_2O_3 coatings. The presence of yttrium (Y) peaks in Ni-B-Y_2O_3 composite spectrum clearly confirms the successful incorporation of particles in the nickel matrix. Furthermore, change in the metallic luster of Ni-B coatings is also noticed by the incorporation of Y_2O_3 particles. Although, the phenomenon of co-deposition of boron in the Ni matrix through the electrodeposition process is not yet well understood, it is anticipated that co-deposition of

boron into Ni matrix takes place because of adsorption of dimethylamine borane complex (DMAB) used as a source of boron in this study. The addition of Y_2O_3 into Ni-B matrix is resulted firstly because of nickel ions absorbing at the Y_2O_3 particle surface. These particles diffuse in the second step due to their ionic cloud which is close to the cathode and a poor adhesion of Y_2O_3 particles on the surface of the substrate (cathode) is possible with the diffusion layer. Towards the completion of the incorporation process, nickel ions are discharged at the substrate surface and the already adhered Y_2O_3 particles are entrenched into the Ni-B matrix [10].

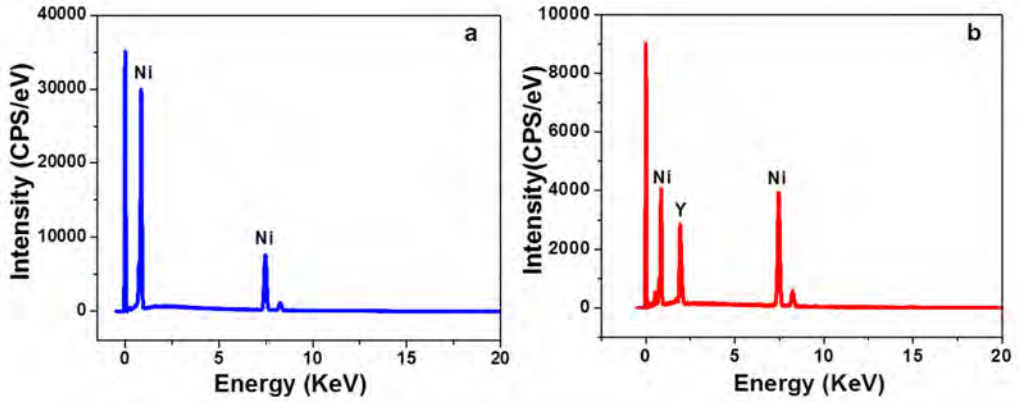

Figure 2. EDX analysis of electrodeposited Ni-B (**a**) and Ni-B-Y_2O_3 (**b**) composite coatings.

3.2. Surface Morphology

Surface analysis of electrodeposited Ni-B and Ni-B-Y_2O_3 coatings has been carried out through FESEM and AFM. Morphology of the coatings significantly affects the performance of the coatings. Figure 3 presents the FESEM analysis of Ni-B (a) and Ni-B-Y_2O_3 composite coatings (b) in their as deposited state.

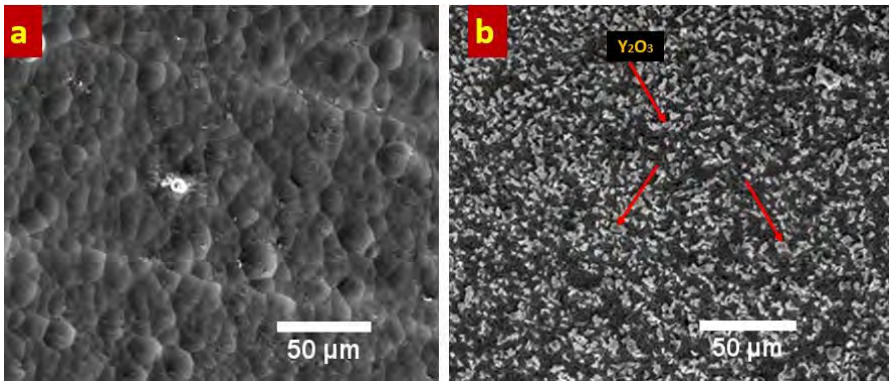

Figure 3. Coating morphology; FESEM images of electrodeposited Ni-B (**a**) and Ni-B-Y_2O_3 composite coatings with arrowheads indicating incorporated Y_2O_3 particles (**b**).

The results show that electrodeposition has produced intact coatings which are free of surface defects including pores and cracks. It also reveals that very homogenous, and dense coatings were developed. Such morphological features are highly desirable as the corrosion phenomenon is highly reduced by restricting the permeation of water and other solvents towards the underlying metal substrate. The presence of Y_2O_3 particles can be clearly noticed in the Ni-B matrix, Figure 3b. The particles are uniformly and evenly distributed throughout the Ni-B matrix which will ensure stable and homogeneous properties throughout the entire span of coatings. It is also observed that no agglomeration of particles happened suggesting that the selected stirring rate was sufficient to maintain the uniform dispersion of particles in the salt bath during the coating deposition. Addition of ceramic particles in the Ni-B matrix usually leads to improve their mechanical characteristics [1,4,11,13].

Interestingly, addition of insoluble, hard Y_2O_3 particles have resulted in significant grain refinement of the Ni-B matrix which also leads to enhance the mechanical and electrochemical behavior of the coatings. The incorporation of Y_2O_3 particles is believed to facilitate the prevention of grain growth at the surface of cathode which ultimately results in the grain size refinement of the nickel matrix [4]. This observation is in agreement with our grain size calculations based on XRD analysis presented in Figure 1.

Morphology of the developed coatings was further studied through Atomic Force Microscopy (AFM) and 3D images are presented in Figure 4. The current results strongly support the FESEM analysis confirming that the grain size has been refined with introduction of Y_2O_3 particles into the coating bath for Ni-B-Y_2O_3 composite coatings. It can be figured out that Ni-B coatings have larger nodular structure when compared to Ni-B-Y_2O_3 composite coatings. Moreover, the presence of Y_2O_3 particles can be clearly seen in the Ni-B-Y_2O_3 coatings (Figure 4b). This outcome reveals that incorporation of Y_2O_3 ceramic particles into the Ni-B matrix have resulted in significant alteration of coating morphology. The surface morphology was also studied quantitatively in terms of root-mean-square roughness (RMS) which is described as the average height deviation from the reference line. The surface roughness analysis of Ni-B and Ni-B-Y_2O_3 composite coatings indicates that Ni-B coatings have higher RMS value (27.872 nm) when compared to the Ni-B-Y_2O_3 composite coatings (7.834 nm). The alteration of surface roughness presumably can be considered the effect of grain refinement by the addition of Y_2O_3 into Ni-B matrix. Furthermore, the AFM analysis confirms that the developed coatings are free of defects such as cracks and pores, etc. supporting the observations made through FESEM.

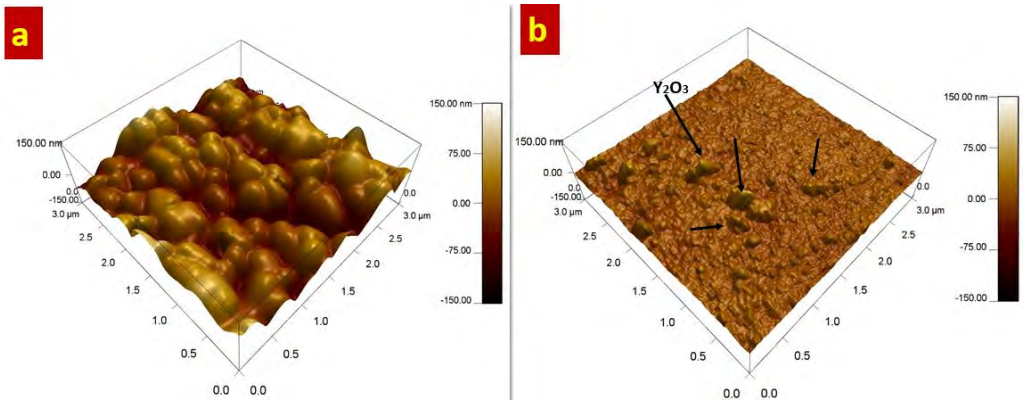

Figure 4. Coating morphology; AFM images of electrodeposited Ni-B (**a**) and Ni-B-Y_2O_3 composite coatings with arrowheads indicating incorporated Y_2O_3 particles (**b**).

3.3. Thermal Properties

Thermal properties of Ni-B and Ni-B-Y_2O_3 composite coatings were studied by using DSC analysis and the results are shown in Figure 5.

It can be clearly observed that the substrate material maintains smooth spectrum up to the examined temperature range, revealing the absence of any phase changes. On the other hand, two exothermic peaks are observed at 593 K (320 °C) and 635 K (362 °C) for Ni-B coatings which indicate two different phase transformations. The phase changes observed at 593 K (320 °C) in Ni-B coatings may correspond to the re-crystallization of nickel and the formation of Ni_3B phases into the nickel matrix. On the other hand, the presence of an exothermic peak at 635 K (362 °C) might be assigned to the nucleation of Ni_3B_4 [1,9]. In contrast, a single exothermic peak is observed at 648 K (375 °C) in the Ni-B-Y_2O_3 composite layer, which might correspond to the formation of Ni_3B_4 into the nickel matrix. This results indicate that the addition of Y_2O_3 in to the Ni-B matrix has suppressed the first transformation at 593 K (320 °C) occurring in Ni-B coatings, confirming the improved thermal stability of Ni-B matrix.

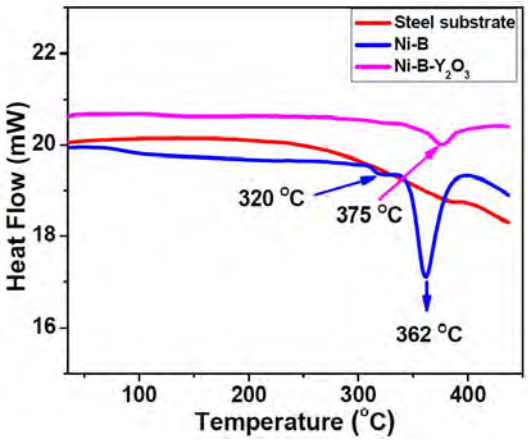

Figure 5. Thermal analysis of electrodeposited Ni-B and Ni-B-Y_2O_3 composite coatings.

3.4. Mechanical Properties

The mechanical behavior of Ni-B and Ni-B-Y_2O_3 composite coatings was studied through nanoindentation. The loading and unloading profiles of nanoindentation for the comparative analysis of Ni-B and Ni-B-Y_2O_3 coatings are presented in Figure 6.

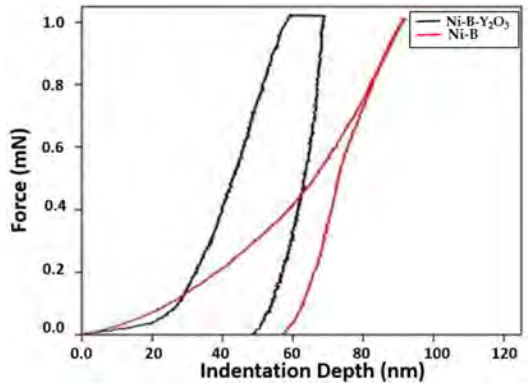

Figure 6. Loading/unloading nanoindentation profiles for Ni-B and Ni-B-Y_2O_3 electrodeposited composite coatings.

Two parameters are important here; the area under the curve for each coating and the depth of penetration. The area under the curve of Ni-B is larger as compared to Ni-B-Y_2O_3 composite coatings. The depth of penetration is also larger in case of Ni-B coatings when compared with Ni-B-Y_2O_3 composite coatings which suggests the lower hardness and strength of Ni-B coatings as compared to Ni-B-Y_2O_3 composite coatings. Higher indentation depth of ~58 nm was achieved for Ni-B coatings, whereas Ni-B-Y_2O_3 composite coatings showed ~50 nm suggesting superior resistance to indentation and thus improved mechanical response. Previously, different research groups have reported similar trends, supporting the idea of mechanical properties enhancement of coatings with incorporation of reinforcing particles [18]. The graphs also reveal that the Ni-B-Y_2O_3 deposited coatings possess kinks which are not visible for Ni-B coatings. The origination of such kinks are attributed to the presence of pores or multiphase structure of the coatings. When pores are present in the coatings, then a microcollapse might occur underneath the indentor, resulting in an abrupt variation in the stress–strain analysis. Similarly, when a second phase particle is scanned by the indentor, then fluctuation occurs in the slope of the load-displacement profile of nanoindentation [19]. The mentioned mechanism is well followed by the current results as the Ni-B coatings showed a profile smooth and free of kinks. However, kinks were observed in the nanoindentation profiles of Ni-B-Y_2O_3 composite coatings due to the introduction of second phase reinforcing particles.

The loading and unloading profiles of nanoindentation tests were also utilized to conduct quantitative analysis for the calculation of the mechanical properties listed in Table 2 (hardness, modulus of elasticity, stiffness, and plasticity).

Table 2. Calculated mechanical properties of Ni-B and Ni-B-Y_2O_3 composite coatings.

Nomenclature	Hardness (GPa)	Modulus of Elasticity (E_c) (GPa)	Stiffness (kN/m)	Plasticity
Ni-B	8.98	97.60	40.37	1.50
Ni-B-Y_2O_3	15.99	287.88	85.23	0.55

The hardness of synthesized coatings was determined by the Oliver Pharr method which was explained in detail in our previous published work [4]. We observed a remarkable improvement in mechanical properties of Ni-B coatings by the incorporation of Y_2O_3 into Ni-B matrix. The hardness of Ni-B matrix was significantly increased by ~79%. Similarly, the modulus of elasticity (~195%) and stiffness (~111%) of Ni-B matrix have been remarkably increased with addition of Y_2O_3 reinforcing particles. The improvement in the modulus of elasticity is attributed to the hard and brittle Y_2O_3 particles. These particles act as strong reinforcements throughout the Ni-B matrix. It leads to producing coatings with characteristics of high hardness/strength and low elongation (strain), thus resulting in the increased modulus of elasticity. The enhancement in modulus of elasticity and hardness is due to the addition of hard ceramic phase leading to dispersion hardening effect as reported in the literature. During the dispersion hardening process, the presence of Y_2O_3 particles into the Ni-B matrix impedes the motion of the dislocations and thus the restraining of dislocations at the Y_2O_3 particles leads to the enhancement in mechanical properties [1,10,11,13]. The enhancement in hardness of the Ni-B matrix by incorporation of Y_2O_3 particles can also be explained by the rule of mixtures [20], being presented as Equation (2).

$$H_C = H_m F_m + H_r F_r \quad (2)$$

where, H_m, H_r, and H_c are the hardness of the matrix, reinforcement and composite, whereas the F_r, and F_m are the volume fraction of reinforcement and the matrix, respectively. Since, Y_2O_3 particles have high hardness so their addition to Ni-B matrix improves its hardness.

3.5. Corrosion Behavior

The potentiodynamic polarization experiments of the electrodeposited coatings were conducted using a Gamry Reference Eco potentiostat at a scan rate of 10 mV·min^{-1} (0.167 mV·s^{-1}). The potentiodynamic curves of steel substrate, Ni-B and Ni-B-Y_2O_3 composite coatings are presented in Figure 7. The potentiodynamic curve for steel substrate is included for comparison.

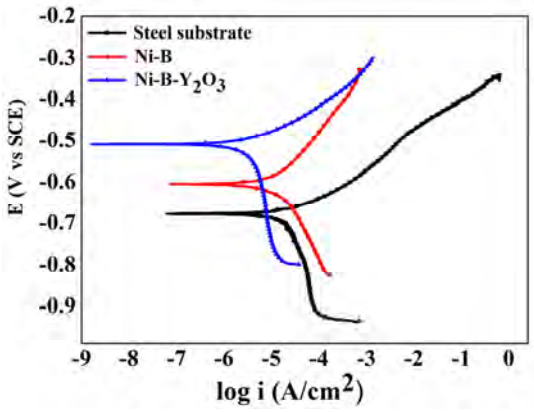

Figure 7. Potentiodynamic polarization of Ni-B-Y_2O_3 composite coatings in 3.5 wt % NaCl aqueous solution at the scan rate of 0.167 mV·s^{-1}.

i_{corr}, β_a, β_c, E_{corr}, and protection efficiency has been calculated from the potentiodynamic polarization curves and are presented in Table 3. The steel substrate and Ni-B showed corrosion current densities of 26.2 $\mu A/cm^2$ and 19.3 $\mu A/cm^2$, respectively. However, it becomes clearly evident that incorporation of reinforcing Y_2O_3 particles greatly enhances the corrosion resistance of Ni-B matrix. Corrosion current density of Ni-B-Y_2O_3 composite coatings is significantly reduced to 6.9 $\mu A/cm^2$. Such a low value of current density confirms decent corrosion resistance of Ni-B-Y_2O_3 composite coatings. The corrosion protection efficiency of coatings was calculated by using Equation (3) [21].

$$\text{Efficiency} = 1 - \frac{i_2}{i_1} \times 100\% \quad (3)$$

i_1 and i_2 represents the corrosion current densities of the bare substrate and coated samples, respectively. The positive influence of Y_2O_3 particles addition to coatings can be understood by the fact that the corrosion protection efficiency of Ni-B-Y_2O_3 coatings is improved to ~74% which is ~48% higher than that of the Ni-B coatings (26%). The enhanced corrosion efficiency of Ni-B-Y_2O_3 composite coatings is believed to be because of the decrease in the active area of Ni-B matrix. The addition of hard and inert Y_2O_3 particles reduces the active sites on the coating surface for Cl^- ion adsorption, and thus the corrosion resistance is improved [1,4,8].

Table 3. Potentiodynamic polarization parameters of steel substrate, Ni-B and Ni-B-Y_2O_3 composite coatings determined in 3.5 wt % NaCl aqueous solution under the scan rate of 0.167 $mV \cdot s^{-1}$.

Nomenclature	E_{corr} (V)	i_{corr} (μA)/cm^2	β_a ($mV \cdot dec^{-1}$)	β_c ($mV \cdot dec^{-1}$)	Protection Efficiency (%)
Steel Substrate	−0.7	26.2	74.8	467.7	–
Ni-B	−0.6	19.3	64.4	268.3	26.3
Ni-B-Y_2O_3	−0.5	6.9	72.3	822.6	73.6

Although, there is improvement in mechanical and anticorrosion properties of Ni-B coatings by the addition of Y_2O_3 particles, we believe that the properties of Ni-B-Y_2O_3 composite coatings can be further improved using Y_2O_3 nanoparticles and adopting pulse electrodeposition process instead of the conventional electrodeposition process.

4. Conclusions

The electrodeposition process was used to synthesize Ni-B and Ni-B-Y_2O_3 coatings. Addition of Y_2O_3 particles to the Ni-B matrix has considerable effect on its structure, surface, thermal, mechanical, and anticorrosion properties. Incorporation of Y_2O_3 particles into the Ni-B matrix increases its crystallinity and refines the grain size. Addition of Y_2O_3 particles into the Ni-B matrix also improves its mechanical properties which can be mainly ascribed to the grain refinement and dispersion hardening effect due to the presence of hard Y_2O_3 particles. Finally, the potentiodynamic results confirm that Ni-B-Y_2O_3 composite coatings demonstrate superior protection efficiency (~74%) when compared to Ni-B coatings (~26%). Owing to their improved mechanical and anticorrosion properties, the Ni-B-Y_2O_3 composite coatings may find their potential applications in industries including oil and gas, automobile, seawater desalination, and many others.

Acknowledgments: This publication was made possible by NPRP Grant NPRP-9-080-2-039 from Qatar National Research Fund (a member of the Qatar Foundation). Statements made herein are solely the responsibility of the authors.

Author Contributions: R.A.S. proposed the basic idea of the current research work, supervised the whole research work, participated in technical discussions, and finalized the contents of the manuscript after successive revisions. U.S.W. prepared Ni-B and Ni-B-Y_2O_3 composite coatings after optimizing coating synthesis conditions. K.A. performed corrosion analysis of Ni-B and Ni-B-Y_2O_3 composite coatings and prepared the manuscript. R.K. supervised the corrosion tests, revised the manuscript, and participated in technical discussion. A.P. conducted nanoindentation tests of the developed coatings. M.M.Y. performed AFM analysis of the synthesized coatings. A.H. conducted SEM/EDX analysis of the coatings and reviewed the prepared manuscript.

Conflicts of Interest: The authors declare no conflict of interest.

References

1. Shakoor, R.A.; Kahraman, R.; Waware, U.S.; Wang, Y.; Gao, W. Properties of electrodeposited Ni-B-Al_2O_3 composite coatings. *Mater. Des.* **2014**, *64*, 127–135. [CrossRef]
2. Shakoor, R.A.; Kahraman, R.; Waware, U.S.; Wang, Y.; Gao, W. Synthesis and properties of electrodeposited Ni-B-CeO_2 composite coatings. *Mater. Des.* **2014**, *59*, 421–429. [CrossRef]
3. Boccaccini, A.R.; Zhitomirsky, I. Application of electrophoretic and electrolytic deposition techniques in ceramics processing. *Curr. Opin. Solid State Mater. Sci.* **2002**, *6*, 251–260. [CrossRef]
4. Radwan, A.B.; Shakoor, R.A.; Popelka, A. Improvement in properties of Ni-B coatings by the addition of mixed oxide nanoparticles. *Int. J. Electrochem. Sci.* **2015**, *10*, 7548–7562.
5. Bekish, Y.N.; Poznyak, S.K.; Tsybulskaya, L.S.; Gaevskaya, T.V. Electrodeposited Ni-B alloy coatings: Structure, corrosion resistance and mechanical properties. *Electrochim. Acta* **2010**, *55*, 2223–2231. [CrossRef]
6. Shakoor, R.A.; Kahraman, R.; Waware, U.S.; Wang, Y.; Gao, W. Synthesis and properties of electrodeposited Ni-B-Zn ternary alloy coatings. *Int. J. Electrochem. Sci.* **2014**, *9*, 5520–5536.
7. Krishnaveni, K.; Narayanan, T.S.N.S.; Seshadri, S.K. Corrosion resistance of electrodeposited Ni-B and Ni-B-Si_3N_4 composite coatings. *J. Alloys Compd.* **2009**, *480*, 765–770. [CrossRef]
8. Shakoor, R.A.; Kahraman, R.; Waware, U.S.; Wang, Y.; Gao, W. Properties of electrodeposited Ni-B-ZrO_2 composite coatings. *Int. J. Electrochem. Sci.* **2015**, *10*, 2110–2119.
9. Krishnaveni, K.; Narayanan, T.S.N.S.; Seshadri, S.K. Electrodeposited Ni-B coatings: Formation and evaluation of hardness and wear resistance. *Mater. Chem. Phys.* **2006**, *99*, 300–308. [CrossRef]
10. Krishnaveni, K.; Narayanan, T.S.N.S.; Seshadri, S.K. Electrodeposited Ni-B-Si_3N_4 composite coating: Preparation and evaluation of its characteristic properties. *J. Alloys Compd.* **2008**, *466*, 412–420. [CrossRef]
11. Wang, Y.; Wang, S.J.; Shu, X.; Gao, W.; Lu, W.; Yan, B. Preparation and property of sol-enhanced Ni-B-TiO_2 nano-composite coatings. *J. Alloys Compd.* **2014**, *617*, 472–478. [CrossRef]
12. Niksefat, V.; Ghorbani, M. Mechanical and electrochemical properties of ultrasonic-assisted electroless deposition of Ni-B-TiO_2 composite coatings. *J. Alloys Compd.* **2015**, *633*, 127–136. [CrossRef]
13. Ogihara, H.; Wang, H.; Saji, T. Electrodeposition of Ni-B/SiC composite films with high hardness and wear resistance. *Appl. Surf. Sci.* **2014**, *296*, 108–113. [CrossRef]
14. Okonkwo, P.C.; Shakoor, R.A.; Benamor, A.; Mohamed, A.M.A.; Al-Marri, M.J.F.A. Corrosion behavior of API X100 steel material in a hydrogen sulfide environment. *Metals* **2017**, *7*, 109. [CrossRef]
15. Yang, Q.; He, Y.; Fan, Y.; Zhan, Y.; Tang, Y. Effect of β-cyclodextrin as organic additive on pulse electrodeposition of nanocrystalline Ni-W coating. *Int. J. Electrochem. Sci.* **2016**, *11*, 5103–5110. [CrossRef]
16. Gyawali, G.; Cho, S.H.; Lee, S.W. Electrodeposition and characterization of Ni-TiB_2 composite coatings. *Met. Mater. Int.* **2013**, *19*, 113–118. [CrossRef]
17. Gyawali, G.; Lee, S.W. Effect of SiC and h/BN codeposition on microstructural and tribological properties of Ni-SiC-h/BN composite coatings. *J. Ceram. Process. Res.* **2015**, *16*, 213–217.
18. Temam, H.B.; Chala, A.; Rahmane, S. Microhardness and corrosion behavior of Ni–SiC electrodeposited coatings in presence of organic additives. *Surf. Coat. Technol.* **2011**, *205*, S161–S164. [CrossRef]
19. Samiee, F.; Raeissi, K.; Golozar, M.A. Nanoindentation testing of pulse electrodeposited thin zirconia coatings. *Surf. Eng.* **2013**, *29*, 726–730. [CrossRef]
20. Roy, R.; Agrawal, D.; Cheng, J.P.; Mathis, M. Microwave processing: Triumph of applications-driven science in WC-composites and ferroictitanates. *Ceram. Trans.* **1997**, *80*, 3–26.
21. Yuan, S.; Pehkonen, S.O.; Liang, B.; Ting, Y.P.; Neoh, K.G.; Kang, E.T. Superhydrophobic fluoropolymer-modified copper surface via surface graft polymerisation for corrosion protection. *Corros. Sci.* **2011**, *53*, 2738–2747. [CrossRef]

© 2017 by the authors. Licensee MDPI, Basel, Switzerland. This article is an open access article distributed under the terms and conditions of the Creative Commons Attribution (CC BY) license (http://creativecommons.org/licenses/by/4.0/).